Mater Eng Res, 2019, 1(1): 20-31
DOI: 10.25082/MER.2019.01.005

RESEARCH ARTICLE

A study on the deformation and crushing of copper tubing: experiments, theory & FE modelling

R.P. Turner

Abstract: A series of 250 mm lengths of copper tubing, of 15 mm outer diameter and 0.7 mm wall thickness, were studied to determine their deformation if they were pinched or crushed between rigid objects applying a given force, to replicate potential accidental damage suffered by the copper pipes during service. A finite element modelling framework was developed to simulate the crushing of a copper pipe the same dimensions as that used for experiments, and the experimental data allowed for a validation of the pipe crushing at approximately room temperature, to consider copper pipe carrying cold water. The FE modelling activity was then extended to consider the deformation of copper pipe at 80°C, carrying heated water at this temperature. The modelling agreed reasonably well with experiment, and applied forces of 1.5 kN began to deform the cold pipe, with the pipe collapsing on itself at loads of 6 kN. The heated pipe began to deform at roughly 1.25 kN. Lastly, theoretical flow calculations were performed to determine the Reynolds value, the flow velocity and the pressure loss and head loss per unit length of the deformed pipes, according to classical pipe flow calculation methods.

Keywords: simulation, fluid mechanics, finite element, pressure drop

1 Introduction

Copper tubing is commercially available as standard in all sorts of pipe diameter sizes, ranging from a small, thin walled pipe of 15 mm diameter and wall thickness 0.7 mm, to 80 mm diameter and approximately 2.0 mm wall thickness, for commercial plumbing requirements[1] . Typical uses for copper tubing include the supply of cold and heated water from a mains water line to a local tap or boiler unit[2] , or as a refrigerant fluid transportation line in a heating, ventilation and air-conditioning (HVAC) system[3] . Copper is used to produce these fluid (often water) carrying pipes for a number of reasons. It is anti-microbial (employing the oligodynamic effect)[4] , which can kills bacteria before build-up[4] , it generally does not leach harmful metals in to the fluid it carries, as opposed to some other metals that can much more readily leach out in to the fluid[5] , it is non-permeable[6] , it does not suffer from corrosion readily in the typical working environment[7] , it is a ductile metal that can be shaped more readily than other metals, and its ductility offers greater fracture toughness than some other metals[8] . It is also an abundant natural resource[2] , and further is readily recyclable, thus reducing the raw material costs.

However, it is the material's malleability at moderate temperatures[6] to allow for ease of pipe manipulation which is the predominant reason that it is so widely used. Yet, copper's relative malleability at low temperatures may also be considered a weakness of the material, as it does mean that the pipe is susceptible to sustaining damage whilst in-service, through accidental impact or through undesired trapping mechanisms whilst in service.

The raw copper material can come from either virgin or recycled copper routes, however copper is one of the most recycled metals, and the copper scrap is often obtained from stripping down industrially used copper electrical wire to the bare wire component. Recycled copper generally shows very little degradation of mechanical property[9] , along with the usual impact of recycling including concomitant environmental and cost benefits, meaning recycled copper is increasingly in demand[10] .

Copper is a FCC lattice structure, it is a dense metal (8,900 kgm^{-3}) with a melting temperature of 1083°C. It generally is a relatively unreactive metal, with noticeable oxidation only occurring over a period of many years. This oxidation layer, called a patina, actually protects the copper below from further atmospheric degradation, whilst offering minimal reduction in the material prop-

Received: March 27, 2019 **Accepted:** April 17, 2019; **Published:** April 19, 2019

* **Correspondence to**: R.P. Turner, School of Metallurgy & Materials, University of Birmingham, Birmingham B15 2TT, UK; Email: R.P.Turner@bham.ac.uk

Citation: Turner RP. A study on the deformation and crushing of copper tubing: experiments, theory & FE modelling. *Mater Eng Res*, 2019, **1**(1): 20-31.

erty.

Copper tubing is manufactured on a considerable scale, given the widespread use of the finished product across a vast number of industrial applications. In order to manufacture the copper tubing, the raw material must be fed in to a furnace and melted. For common tubing applications, the raw copper comes from high quality grades of recycled scrap copper (sometimes referred to as bare bright copper)[11] . This grade ensures that the recycled material is largely free from contaminants and other material, and free from any visible oxidation. Sections scrap of material eligible to be classed as bare bright copper must be thicker than 16 gauge[11] (approximately 1.59 mm thick).

The raw material copper is melted in a large reverberatory furnace. The melt is raised to approximately 1260 to 1300°C, well in excess of the melt point of copper (1083°C). The molten copper is then fire-refined by the introduction of oxygen, which reacts to form oxides much more readily with any impurities still within the melt[12] . The oxides of the impurities are less dense than the copper, and so float to the surface as slag. Small traces of copper oxide are removed using additions of phosphorus to react with the oxygen, leaving near pure copper. This recycled copper can reach roughly 99.9% purity, virtually as pure as copper produced from virgin ore[12] .

The molten copper is subsequently poured in to horizontally aligned, water-cooled graphite moulds. Grips then pull the now solidified copper log linearly within the mould, allowing space for further molten copper to be poured in to the gap created at the back. The process continues as such until the maximum length of copper log is created. Once the cylindrical log is produced via continuous casting, the copper billet is placed in to an extrusion press. The billet is heated to the required forming temperature, and is pierced using a mandrel. A ram is located at the back end of the extrusion chamber, forcing the heated copper over the mandrel and through an extrusion hole on the opposite side of the chamber to the ram. The size and shape of the hole which the heated, highly malleable copper is forced through dictates the extruded material size and shape. The hollow copper tubing that emerges from the extruder can then be drawn out further, using grips to contact the tube, and pulling it through further dies to reduce its outer diameter and its wall thickness to the relevant size required[13] .

The process of drawing serves to work-harden the copper[14] , thus drawn tube has improved material mechanical properties such as the fracture toughness, compared to prior to drawing. Work-hardening is achieved through small amounts of plastic deformation within the materials causing a saturation of dislocations[15] within the crystal structure of the copper.

One of the main advantages of tubing production using this type of extruded and drawn methodology is the seamless nature of the finished product, with homogenous property and microstructure throughout its outer wall, and its wall thickness[13] . As opposed to seamless tube, welded tubing is formed from a flat sheet of material that is subsequently rolled and welded longitudinally. The presence of the weld within rolled, welded tubing can cause in-service issues, especially for pressurised pipe systems. However, despite the extra manufacturing costs associated with the extrusion method compared to rolled and welded, an extruded and drawn seamless tubing component offers improved mechanical properties. Thus, the seamless tubing is desirable within industrial applications, especially when considering the expense and containment issues associated with a burst pipe.

The mechanical properties of copper largely depend upon its route of production; however it does have good toughness at low temperatures, has room temperature strength of roughly 190-250 MPa[16] , which can be further enhanced by cold work-hardening. As the temperature increases, the strength remains roughly constant up to approximately 70°C, before beginning to decrease, with an increasing gradient, up to approximately 200°C. The yield strength decreases very gradually from room temperature up to 200°C.

Finite element simulations concerning the structural integrity of a pipe component are not new, indeed there are numerous instances within the literature of FE or numerical modelling to analyse the structural integrity, strength, and associated residual stress field left behind after pipe welding[17–21] , or through impact and loading[22,23] , however most of these studies tended to be considering steel pipework. Thus, there is a considerable gap in the efforts of FE and numerical analysts to simulate accidental deformation, and the knock-on effect of fluid flow within a damaged pipe, for the copper pipes so prominently used.

2 Material and methods

Copper pipe of external diameter 15 mm, wall thickness of 0. 7 mm, and thus internal diameter of 13.6 mm, was used for experimental measurements of pipe deformation due to certain applied loads. An ESH Testing Ltd 100 kN load frame press was used to apply the fixed load on to the central portion of pipe, which was clamped in-between two jaws measuring 25 mm in width. The set-up can be seen in the schematic given in Figure 1.

The press and jaw arrangement were utilised to apply specified loads to the pipe, in order to crush the pipe, as a physical simulation of a pipe becoming trapped in service and deforming accordingly. The applied loads were, in increasing order; 1.5 kN, 2 kN, 2.5 kN, 3 kN and 6 kN. There was no further clamping, lubrication or equipment used. The bar and jaws were at a constant 15-20°C, as was the surrounding atmosphere at the room temperature of the laboratory, in order to replicate the cold pipe under service.

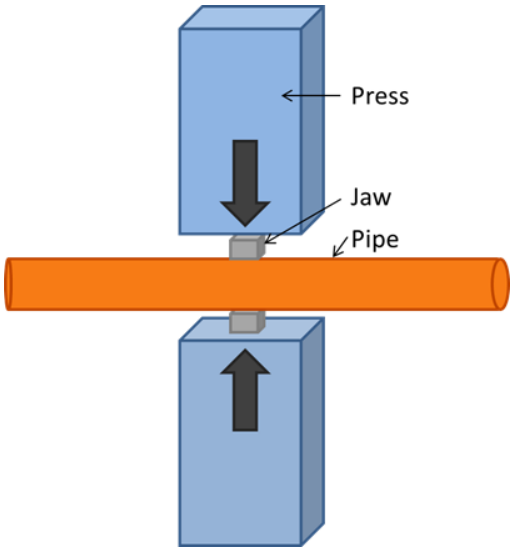

Figure 1. A schematic diagram showing the experimental set-up for deforming the pipe

3 Finite element modelling

An FE model was constructed using the Deform v11.2 software, from software developers SFTC[24] . The model was created using various rigid and plastically deformable objects. A plastically deformable workpiece was employed to represent the copper pipe. The model simulated a copper pipe of length 250 mm, with 15 mm outer pipe diameter and wall thickness of 0.7 mm. This was meshed by initially meshing the 2D cross-section of the pipe-wall with 2D quadrilateral elements, and then extruded through the length of the pipe to produce the 3D component. Hence, the elements were hexahedral, and numbered about 25,000 in the deformable workpiece.

The 3D pipe workpiece was assigned the properties of the copper material, with a Young's Modulus of 115GPa (at 15°C) or 105 GPa (at 80°C), a Poisson ratio of 0.33 and a temperature dependent flow stress given by the simplified Johnson-Cook Equation:

$$\bar{\sigma} = (A + B\bar{\epsilon}^{n}) \left[1 + C.ln\left(\frac{\dot{\epsilon}}{\dot{\epsilon_0}}\right)\right] (1 - (T^*)^m) \quad (1a)$$

Where

$$T^* = \frac{T - T_{rm}}{T_{melt} - T_{rm}} \quad (1b)$$

And where $\bar{\epsilon}$ is the mean strain, $\dot{\epsilon}$the mean strain rate, T is operating temperature, $T_{rm}$is room temperature (15°C) and T_{melt} is melting temperature (1085°C),with further material dependent parameters *A, B, C, m, n,* $\dot{\epsilon_0}$ to be defined. In the case of copper, the values used are as given in Table 1.

These parameters to be fitted to match the material behaviour can largely be purely numerically quantified with little physical meaning, however analysing the form of the equation can inform that $\dot{\epsilon_0}$ is a reference strain rate, n is an exponent for the strain hardening, m is an exponent for the high temperature softening, and A is the base flow stress value when at room temperature, reference strain rate and zero strain.

Table 1. Parameters used to define the simplified Johnson-Cook flow stress equation

A	B	C	m	n	$\dot{\epsilon_0}$
123.7	435.1	0.022	0.83	0.31	1

Rigid (tooling) objects were used to apply a deformation within the FE model to match the experimental set-up accurately. Thus, cuboid blocks were created to represent the jaws of the compressing tooling that was used to provide the deforming force. As rigid objects experience no deformation, thus these did not require meshing. Boundary conditions between workpiece and rigid tooling, applied at nodes within the workpiece mesh that were in contact with a rigid object were assigned with a shear friction coefficient of 0.08, as is recommended for cold forging operations. The workpiece was also given a self-contact boundary condition for when the pipe inner walls fold and contact. A time step of 0.01 s was implemented, and automatic re-meshing of the workpiece was switched on. The set-up of the model can be seen in Figure 2.

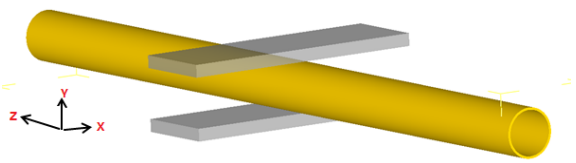

Figure 2. The FE modelling set-up, with the plastically deformable workpiece pipe, and rigid tooling

Two models, identical in set-up barring the pipe workpiece operating temperature were set up. The models were ran in an adiabatic manner, thus heat transfer effects

were neglected and only the mechanical response calculated, and the pipe assumed to remain at the same fixed temperature (either 15°C to represent a cold fluid carrying pipe, and 80°C to represent a hot fluid carrying pipe). This was considered a fair simplification given the pipe will remain at the temperature of the fluid carried during the pipe collapsing procedure, with additional heating due to deformation minimal and thus neglected.

A normalised Cockroft and Latham damage criterion was implemented within the plastically deforming workpiece to simulate the potential for fracture at regions of high strain and stress, to keep a through process track of the evolution of this damage parameter indicating the material likelihood to fracture. The normalised Cockroft and Latham parameter, C_n, is expressed as given in Equation 2.

$$C_n = \int^{\bar{\epsilon}} \frac{\sigma_{max}}{\sigma_{eff}} d\bar{\epsilon_p} \qquad (2)$$

Whereby; σ_{max} is the maximum principal stress, σ_{eff} is the effective (Von Mises) stress, and $\bar{\epsilon_p}$ is the effective plastic strain. The normalising parameter in this equation is the effective stress, and this allows for a fracture likelihood parameter, Cn, to be postulated. No value was set to initiate element deletion; instead the model was allowed to simply accrue damage at locations of likely high stress and strain to give an idea of probable damage sites within the workpiece.

4 Results and Discussion

4.1 Shape

The resulting deformed pipe cross-sectional shapes at different applied loads, predicted using FE software, were critically compared to the experimentally observed pipe cross-sectional shape, to determine the accuracy of the modelling approach. The resulting pipe cross-sections for the cold pipe can be seen in Figure 3(A),3(B).

In the experiment (see Figure 3(B)), the pipe is deforming reasonably consistently with an elliptical mode. At the 2.5 kN load, a "flat" section appears on the top and bottom surfaces, where the apex location had been before. At higher loads, this flat actually turns inward, such that the location along the vertical centre of the pipe will come in to contact first. This central contact is achieved at the 6 kN load experiment, whereby the pipe has collapsed on to itself along its vertical centre-line. Thus, in the experiment, the elliptical mode of deformation is a reasonable approximation up until a force of greater than 3 kN.

For the FE model, the inverting of the pipe wall at the

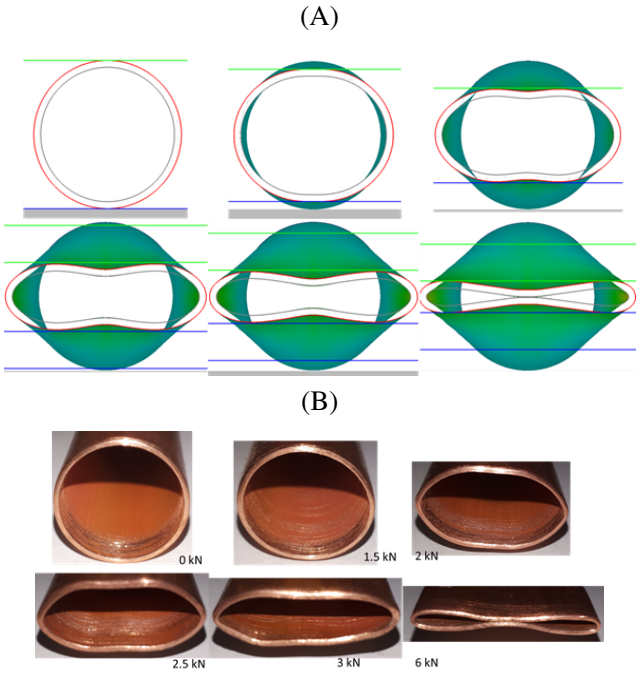

Figure 3. **(A)** Shape predictions for the cold (15°C) pipe at: (1) un-deformed; (2) 1.5kN; (3) 2kN; (4) 2.5kN; (5) 3kN; (6) 6kN **(B)** Experimentally observed pipe deformation shapes at: (1) un-deformed; (2) 1.5kN; (3) 2kN; (4) 2.5kN; (5) 3kN; (6) 6kN

vertical apex locations, such that they turn in toward one another, is predicted to occur at a lower applied load. This is manifested within the 2.5 kN load model, and then continues to become more pronounced until contact is reached, somewhere in between the 3 kN and 6 kN loads. Whilst the applied load at which this first begins is not in agreement with the experiment, the overall trend is correctly predicted. However, it must be stressed that for the FE model, the elliptical deformation mode has broken down for much of the deformation.

The FE modelling framework was extended to also consider the deformation of the same set-up of FE model, but considering a pipe held at a heated 80°C (see Figure 4). This is performed in order to simulate the deformation experienced upon a hot water carrying pipe, where the copper material will have a slightly different mechanical response than when cold (15°C). Again, the trend is shown for an initial elliptical deformation mode to give way to a deformation mode whereby the upper and lower apex locations "turn-in" to produce a slightly narrowed section at the vertical centreline of the pipe.

4.2 Force

The FE model can be interrogated to generate a force vs die separation plot, to predict the collapse pf the pipe under increasing applied loads. The die separation, by definition of the problem, is simply the "height" of the

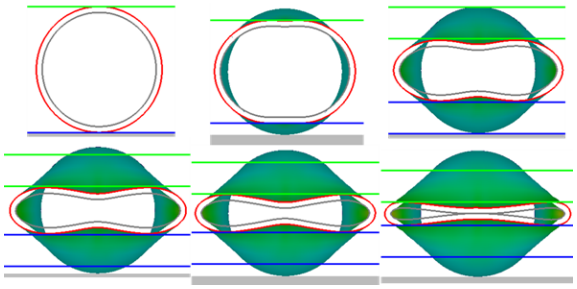

Figure 4. Shape predictions for heated (85°C) pipe at: (1) undeformed; (2) 1.5kN; (3) 2kN; (4) 2.5kN; (5) 3kN; (6) 6kN

deforming pipe in the vertical axis, in-between the tooling applying the loading. The predicted die separation for a given applied force, for the models simulating a cold fluid carrying pipe at 15°C, and for simulating a heated fluid carrying pipe at 80°C can be seen in Figure 5.

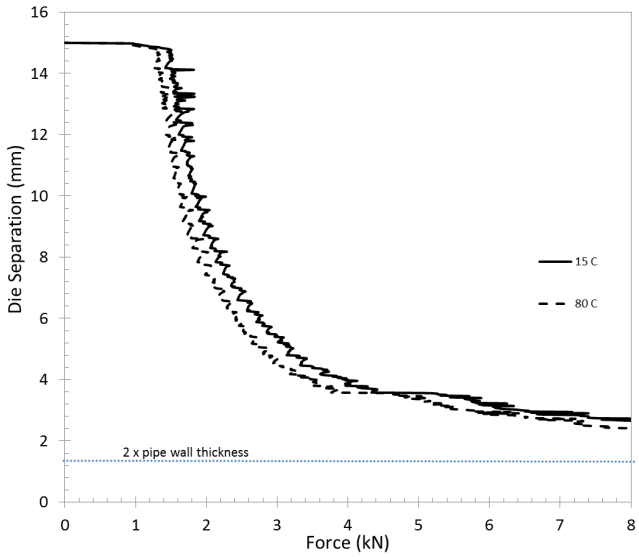

Figure 5. Die separation versus corresponding applied force graph, to illustrate the gradual collapse of the pipe

The onset of deformation of the pipe can be seen to occur for the cold pipe at approximately 1.5 kN, whereas for the heated pipe, this deformation initiates at approximately 1.25 kN. Thus, there is evidently some flow softening of the copper at 80°C compared to 15°C, given that for the same applied load the pipe is deformed more, hence the two dies are closer together.

The resulting semi-minor axis length of the pipe (which by definition is half of the die separation value, measured vertically in the set-up) continues to decrease approximately linearly between 1.5 kN and 2 kN (for the cold pipe) or between 1.25 kN and 1.75 kN (for the 80°C heated pipe), when the reduction in semi-minor axis begin to slow down. As the pipe becomes more plastically distorted, increasing applied loads continue to increase deformation within the pipe, but to a smaller effect, as the deformation approaches a natural asymptote, namely the thickness of two pipe walls for when the pipe has entirely flattened out upon itself, which it cannot be compressed more than.

The pipe deforms initially following the elliptical pipe-wall shape, as shown previously. However, at an applied load of 2 kN, the apex of the upper and lower wall of pipe begin to turn inwards, thus the elliptical description breaks down slightly from this moment onwards. An applied load of 6 kN for the cold pipe model sees these apex positions of upper and lower wall meet. For the heated pipe, this contact of pipe walls occurs at a marginally lower applied force, 5.5 kN. Once the walls contact, the semi-minor axis value (still assuming that one can use an ellipse to describe the pipe, which is not strictly true) decreases a small amount for greater and greater loads, as the pipe is now flattening on to itself.

4.3 Residual stress

The structural integrity of the copper pipe will predominantly depend upon the levels of residual stresses experienced and associated strain within the component, as it is crushed and deformed. It is therefore of interest to be able to analyse these *in-situ* fields of strain and effective (Von Mises) stress across the component during deformation. This capability to perform detailed through-process interrogation of mechanical fields is the primary strength of any FE analysis, if it is assumed that the model has been successfully validated by comparison of shape prediction against experimentally observed deformed pipe shape. Instrumented experimentation to understand the temporally through-process stress and strain fields is extremely challenging, hence the ability to analyse with validated FE tools is a convenient way of understanding how the deformation process influences these mechanical fields.

The Von Mises stress field within the pipe, during differing loads considered, can be seen in Figure 6. Peak Von Mises stresses for the models at the applied loads range from 240 MPa in the 1.5 kN model to 440 MPa in the 6kN model for the cold pipe, and from 240 MPa in the 1.5 kN model to 380 MPa in the 6 kN model for the heated pipe. Whilst the peak stresses did fall approximately 15% in the heated pipe model, it was the difference in Von Mises stress across the central portion of the pipe that saw the greatest decrease when the pipe was heated. At the 6 kN applied force, the modal Von Mises stress value reported at nodes was 250-260 MPa for the cold pipe, whereas it was only 210-220 MPa for the heated pipe, thus the lower banding of predominant

colour in the heated pipe model (see Figure 6).

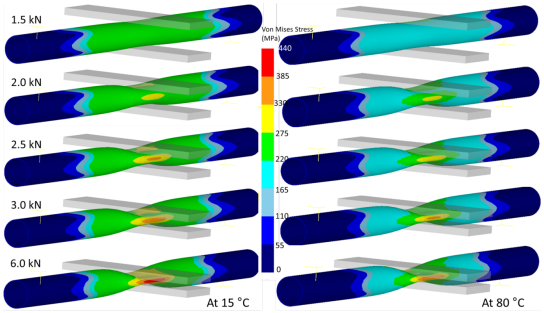

Figure 6. Von Mises residual stress after pipe crushing, at the 5 varying applied loads, for (left) cold 15°C pipe, and (right) heated 80°C pipe

Clearly, the region under the highest stress will be the "shoulder" region of the deformed section of pipe, where the pipe wall is being pushed outward perpendicular to the applied force. However, Von Mises stress does not distinguish between compressive and tensile values. The nature of the stress field can be further interrogated by considering the stress field in the vertical direction (direction of applied load), see Figure 7. For the cold pipe 6 kN applied load model, the pipe cross-section in the X-Z plane through the region of maximum Von Mises stress was analysed.

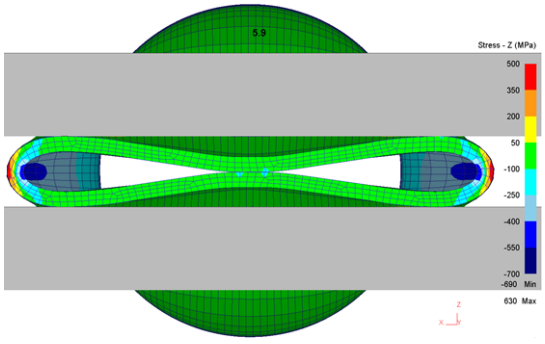

Figure 7. Von Mises residual stress, shown over a cross-section of cold (15°C) pipe for the 6 kN load

The shoulder region experiencing the maximum stress is under a tensile stress field on the outer wall of the pipe, as it is perpendicular to the applied force, whereas the top and bottom of the pipe will experience a compressive stress given these are in the axis of deformation. However, the inner wall, at the location of maximum displacement, must in turn experience a compressive stress, to balance the tensile stress elsewhere. For this highest applied load model (6 kN), the tensile stress in the Z direction on the outer wall reaches similar values to that given by the Von Mises effective stress, approximately 450 MPa, as this is by far the largest contributor in terms of the principal stress axes at this location., thus dominates the equation to calculate Von Mises stress from the principal stress fields. The inner wall sees compressive stresses of a similar magnitude, approximately 470-500 MPa. These predicted peak tensile and compressive stresses fall for the lower applied loads, to approximately 240 MPa (tensile outer wall and compressive inner wall) for the lowest applied load (1.5 kN) for which there is minimal distortion.

4.4 Effective strain

The FE model predicted effective strain fields experienced within the cold and the heated deformed pipe, at the different applied loads, are given in Figure 8. As with the effective stress field, it is clear that the maximum strain will be observed at the shoulder region where the applied load is acting, as this must deform more than any other region in the pipe. The peak effective strain predicted for the models ranges from less than 0.05 for the 1.5 kN applied load, to 0.4 for the 6 kN load. The peak effective strain increases roughly linearly proportionally to the applied load across the 5 models, with an approximate empirically fitted relationship of $\epsilon_{max} = \frac{F\ (kN)}{20}$.

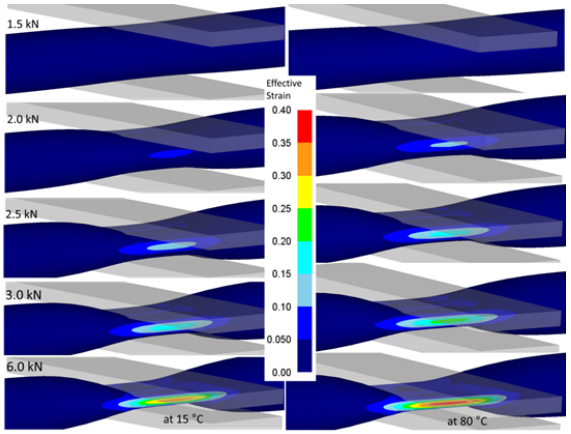

Figure 8. Effective strain for pipes at the 5 varying applied loads; (left) cold 15°C pipe, and (right) heated 80°C pipe

The effective strain field, viewed at the cross-section of the pipe in the X-Z plane, through the point of maximum strain, was analysed. Figure 9 illustrates this cross-sectional view for the 6 kN applied load model, and it is evident that within the predicted strain field, the strain is highest on both the outer and inner walls at the horizontal apex location. Peak effective strain values for the 6 kN applied load are reaching approximately 0 35 on the inner wall, and 0.3 on the outer wall in this plane. The strain reduces to a minimum of roughly half the peak value, at approximately half-way through the 0.7 mm

thick wall.

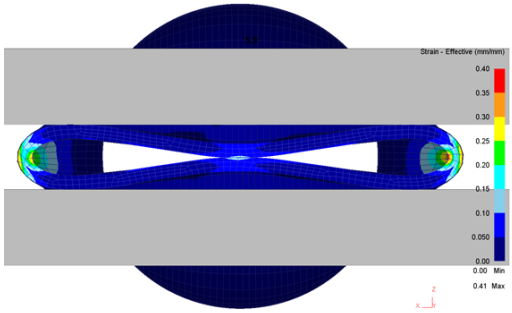

Figure 9. Effective strain, shown over a vertical cross-section of pipe at maximum distortion, for the 6 kN load

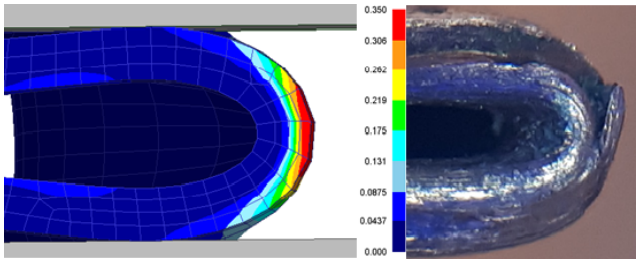

Figure 10. The normalised Cockroft and Latham damage parameter used in the FE model shown as a displayed field over the workpiece, compared to the experimentally observed location of damage

4.5 Fracture / Damage

The FE model can be interrogated to determine the level of "damage" accumulation throughout the pipe, according to the Cockroft and Latham normalised parameter, as defined previously. The maximum accumulation of damage, unsurprisingly given the mathematical description of the parameter, occurs at the outer wall, at the horizontal apex location where the pipe is forming a corner as it begins to fold on to itself.

Figure 10 compares this FE predicted damage parameter against the experimentally observed damage at the same specific location on the pipe which was noted for having peak damage parameter values. Observe that the location of damage observed matches very well with the predicted peak damage in the FE modelling framework. It is therefore considered as further validation of both the damage parameter estimation, and the modelling framework as a whole, that a pure prediction made by modelling has been well-matched against physically observed evidence.

The models were further interrogated to attempt to construct a value for the threshold of normalised Cockroft and Latham damage which will lead to onset of cracking damage within the copper. By considering experimentally observed damage was accumulated somewhere in between the 3 kN and 6 kN applied load, so consultation of these FE models, at the relevant location, suggests a normalised Cockroft and Latham parameter of between 0.25 and 0.35 was the trigger value for the onset of damage.

5 Flow, pressure drop and head loss theory

In order to assess the fitness for purpose of these pipes after suffering the level of deformation experimentally observed and predicted by FE analysis, one must consider the fundamental fluid mechanics, pipe flow, pressure loss and corresponding head loss governing equations. The flow of the fluid being carried by the pipe will depend upon a number of parameters, some associated with the fluid, and some associated with the pipe. As the fluid parameters will be dependent upon temperature, these calculations are performed for both a cold water scenario (15°C) and a hot water scenario (80°C). These calculations are initially performed for the nominal undamaged copper pipe (with perfect circular cross-section), as well as for the 5 examples of deformed pipe cross-sections, as simulated and discussed earlier, for 5 differing loads applied.

One can calculate the relative pipe roughness of the copper pipe using Equation 3, where ϵ is the characteristic surface roughness of copper (estimated to be 0.03 mm), and d the pipe diameter[25] .

$$R = \frac{\epsilon}{d} \tag{3}$$

By making the assumption that the fluid is incompressible, thus we must assume a volumetric flow rate Q is conserved through the process, whereby, for a volumetric flow rate Q, fluid average velocity v and pipe cross section A, the following relationship (Equation 4) holds

$$Q = Av \tag{4}$$

As A will change as the pipe is being deformed, so therefore must v change, to maintain a constant Q. One can calculate the cross-sectional area, assuming that the deformed pipe is represented by a perfect elliptical deformed pipe wall, thus one can calculate v. Note the assumption here that the pipe is deforming as an ellipse, which is a good approximation for lower applied loads to deform, although becomes a worse fit at higher loads. Therefore, one can similarly calculate the Reynolds value of the water flowing in the pipe, using Equation 5[26] .

$$Re = \frac{\rho v d}{\mu} \tag{5}$$

Where ρ is the density of water, v is the flow velocity of the water, and μ is the dynamic viscosity. With calculated values for both the Reynolds value of the moving fluid, and the relative pipe roughness coefficient, the Moody chart can be consulted to understand the Darcy friction factor term of the pipe wall, f_D, as it impedes the flow of the water.

However, when considering the deformed pipe, one must adapt the simplistic formulae, as this is no longer the simple circular cross-section pipe case. In order to calculate relevant properties of the deformed pipe, we will need characteristic dimensions of this non-circular pipe. If we assume the deformed pipe has an elliptical cross section, with a semi-major axis r_α and semi-minor axis r_β, then by using the Ramanujan approximation[27] (Equation 6) we can calculate the pipe circumference.

$$C = \pi \left[3\left(r_\alpha + r_\beta\right) - \sqrt{10 r_\alpha r_\beta + 3\left({r_\alpha}^2 + {r_\beta}^2\right)} \right] \tag{6}$$

In order to calculate the Reynolds value and the relative pipe roughness we require a pipe diameter to be known. In the case of a deformed pipe, we will apply the hydraulic diameter d_H, which is defined in Equation 7[28] :

$$d_H = 4\frac{Area}{wetted\ circumference} = 4\frac{\pi r_\alpha r_\beta}{C} \tag{7}$$

We must then use the hydraulic diameter d_H in place of the diameter d in the equations for effective pipe roughness, pressure drop and head loss. These equations also depend upon the Darcy term f_D, to calculate the pressure drop caused by the frictional resistance of the pipe wall, over a given length (L) of pipe, or to calculate the effective head loss, again over a given length, using Equation 8 and Equation 9[26] , where g is the gravitational acceleration.

$$\frac{\Delta P}{L} = f_D \frac{1}{d_H}\frac{\rho v^2}{2} \tag{8}$$

$$\frac{h_{loss}}{L} = f_D \frac{1}{d_H}\frac{v^2}{2g} \tag{9}$$

The resulting effective circumference, hydraulic diameter, relative pipe roughness, flow velocity, Reynolds value, Darcy friction factor pressure drop and the equivalent head loss values for the pipe as it has undergone different applied loads to deform it can be compared to nominally un-deformed pipe, these values are given in Table 2 and Table 3. For the calculations performed as part of this work, the pipe length is assumed to be 1 metre, thus all expressed pressure drops and equivalent head losses are per metre of damaged, crushed pipe.

The following values are used for cold (15°C) and heated (80°C) water as the fluid of interest. For 15°C water, density ρ = 1000 kgm^{-3}[29] , dynamic viscosity μ = 8.9 x 10^{-4} Pa.s[30] , and the maximum suggested flow velocity for cold water in a non-deformed pipe is 2.4 ms^{-1}, which gives a constant volumetric flow for a 15 mm diameter circular pipe of 0.424 x 10^{-3} m^{3}s^{-1}. For 80°C water, density ρ = 970 kgm^{-3}[29] , dynamic viscosity μ = 3.5 x 10^{-4} Pa.s,[30] and the maximum suggested flow velocity for cold water in a non-deformed pipe is 1.5 ms^{-1}, which gives a constant volumetric flow for a 15mm diameter circular pipe of 0.265 x 10^{-3} m^{3}s^{-1}. The assumed elliptical pipe sections used from the experiment and FE models at different deforming loads were illustrated in Figure 3 and Figure 4.

A cold-fluid carrying pipe, with the fluid and pipe wall held at 15°C (see Table 2), would see the fluid flow velocity increase slightly as the deformation began, as the interior cross-section of the pipe was beginning to reduce, so the flow velocity increases to maintain the constant volumetric flow rate. As the deformation continued and the interior cross-sectional area of the pipe became smaller still, the flow velocity does begin to increase substantially. However, the Reynolds number for the flow remains virtually constant, because it is a function of both the flow velocity and the characteristic distance, namely the pipe hydraulic diameter, which is reducing.

The Darcy friction factor, which is determined using the Moody diagram, remains relativity constant until the pipe relative roughness increases substantially. This increase is in turn caused by the hydraulic diameter reducing significantly to less than half its starting value. It then increases slightly for the highly deformed pipe. Thus, the pressure loss per unit length of pipe, and the corresponding head loss per unit length of distorted pipe, can be calculated. As the pressure loss per unit length of pipe is a function of the Darcy friction factor, the flow velocity squared, and inversely proportional to the hydraulic diameter, so all terms are working to increase the pressure as the pipe becomes more and more deformed. The pressure loss per unit length of pipe for an applied load of 2 kN increases to approximately double the pressure loss for an un-deformed pipe. The pressure loss continues to increase rapidly, becoming severe at a 2.5 kN applied load, and is catastrophic at 6 kN applied load. Similarly, the head loss per unit length of pipe increases such that it is approximately double that of the un-deformed pipe when a 2 kN load is applied, but this head loss increases rapidly for even higher applied loads.

Table 2. Theoretically calculated pipe flow characteristics for the cold 15°C pipe, from first principles

At 15℃	Un-deformed	Deforming Load (kN)				
Pipe / Flow Property	**0**	**1.5**	**2**	**2.5**	**3**	**6**
Semi-major axis (mm)	6.8	7.4	8.6	9.3	9.7	10.2
Semi-minor axis (mm)	6.8	6.0	4.1	2.7	2.0	0.9
Ramanujan Circumference (mm)	42.7	42.0	41.2	40.7	40.9	41.2
Hydraulic diameter (mm)	13.6	13.2	10.8	7.8	5.8	2.8
Relative pipe roughness (-)	0.0022	0.0023	0.0027	0.0038	0.0050	0.0100
Fluid velocity (m/s)	2.9	3.1	3.8	5.4	7.1	14.7
Reynolds value (-)	44,500	45,300	46,200	46,800	46,500	46,100
Darcy friction factor (-)	0.028	0.028	0.028	0.029	0.033	0.040
ΔP (per 1m pipe) (kPa)	8.76	9.97	18.80	53.50	142.40	1545.60
h_{loss} (per 1m pipe) (m)	0.89	1.01	1.91	5.46	14.50	157.80

However, given that the damage caused to a pipe through some type of pinching or crushing action is usually across a narrow section of pipe, almost giving rise to point-damage due to the impact of an external object, so the actual length of the deformed section of pipe is likely very short, of the order of a few centimetres in length, thus the actual pressure drop and head loss over the deformed length of pipe is likely scaled accordingly.

Similar trends are shown for the heated pipe (see Table 3), in that the method of shaping the deformed pipe is very similar to the cold pipe, albeit the distortions are slightly larger for a given applied load, due to the small reduction in flow stresses at this elevated temperature, compared to cold. The hydraulic diameter, calculated from the semi-major and semi-minor lengths, decreases considerably once a load greater than approximately 1.5 kN is applied. As for the cold pipe, it is the significant decrease in hydraulic diameter, which is proportional to the relative roughness term, which causes the major changes in the Darcy friction factor calculation, which increases by roughly a third from the un-deformed pipe value. However, again as with the cold pipe, the fluid flow velocity increase is the critical parameter which dictates the catastrophic pressure and head loss per unit length of deformed pipe.

Figure 11 illustrates the changes calculated in the hydraulic diameter of the pipe, and the resulting pressure drop per unit length of pipe, from the theoretical hand calculations based upon fluid flow within a contained pipe, for different deforming loads applied to the pipe, and at the two different fluid and pipe temperatures. Figure 11 illustrates clearly the beginning of severe reduction in hydraulic diameter as the pipe is deforming, as the theoretically calculated hydraulic diameter suffers a cliff-edge drop off in between 1.5 and 2 kN applied load. Figure 11 illustrates the theoretically calculated increase in pressure drop for increasing deforming load applied to the pipe. This graph is clearly dominated by the relationship with the velocity squared, such that for the relatively linear increase seen in fluid velocity when increasing the applied load from 1.5 kN upwards, the pressure drop increases with a $y=f(x^2)$ type response.

6 Conclusions

A finite element modelling framework has been presented to predict the deformation of 15 mm outer diameter, 0.7 mm wall thickness copper pipes, with tooling

Table 3. Theoretically calculated pipe flow characteristics for the hot 80°C pipe, from first principles

At 80°C	Un-deformed	Deforming Load (kN)				
Pipe / Flow Property	0	1.5	2	2.5	3	6
Semi-major axis (mm)	6.8	7.8	9.3	9.7	10.0	10.3
Semi-minor axis (mm)	6.8	5.4	2.9	2.0	1.6	0.9
Ramanujan Circumference (mm)	42.7	41.8	41.2	41.0	41.3	41.8
Hydraulic diameter (mm)	13.6	13.2	8.3	6.0	4.7	2.6
Relative pipe roughness (-)	0.0022	0.0024	0.0036	0.0050	0.0063	0.0110
Fluid velocity (m/s)	1.8	2	3.1	4.3	5.4	9.6
Reynolds value (-)	68,800	70,200	71,300	71,500	71,100	70,200
Darcy friction factor (-)	0.027	0.027	0.028	0.030	0.032	0.039
ΔP (per 1m pipe) (kPa)	3.20	4.20	15.30	45.60	97.40	660.00
h_{loss} (per 1m pipe) (m)	0.34	0.44	1.61	4.79	10.25	69.15

acting under to apply particular loads to pinch or trap the pipe. Experimental pipe crushing trials were undertaken to validate the modelling approach. In addition, theoretical pipe flow characteristics of the deformed pipes, under different loads, at two different temperatures have been calculated. The following conclusions are drawn:

(1) For cold pipes, an applied force of 1.5 kN will cause an onset of deformation, causing the pipe to begin to become elliptical. The pipe approaches a state of collapse, whereby the upper wall contacts the lower wall, and thus a catastrophic loss of integrity, at an applied load of 6 kN.

(2) Whereas for pipes at 80°C, an applied force of 1.25 kN causes the onset of plastic deformation. However, the reduction in required force compared to the cold pipe remains at approximately the same value of $\frac{1}{4}$ kN lower, thus the heated pipe requires approximately $5\frac{1}{2}$ to $5\frac{3}{4}$ kN deforming load to achieve the same form of collapse as seen in the cold pipe.

(3) The flow of fluid through the piping remains at approximately the same Reynolds value throughout. However, as the pipe deforms, the hydraulic diameter reduces, the required flow velocity increases, and as such the pressure loss per unit length of pipe, and head loss per unit length, increase with a $y = f\,(x^2)$ type response.

(4) The elliptical deformation of the pipes holds reasonably true until a deforming load of 2kN, whereby the top and bottom apex inversion within the deforming pipe becomes substantial compared to the semi-minor axis.

(5) The normalised Cockroft and Latham damage parameter predicted with reasonable accuracy the location of damage observed experimentally on the copper pipe, and an approximate value to initiate macro-scale damage has been estimated as 0.25-0.35.

Acknowledgements

Thanks are offered to the technical support staff at Wilde Analysis, Stockport, UK, for their technical assistance with the FE modelling. Thanks are offered to David Price, in the mechanical testing laboratory, School of Metallurgy & Materials, University of Birmingham.

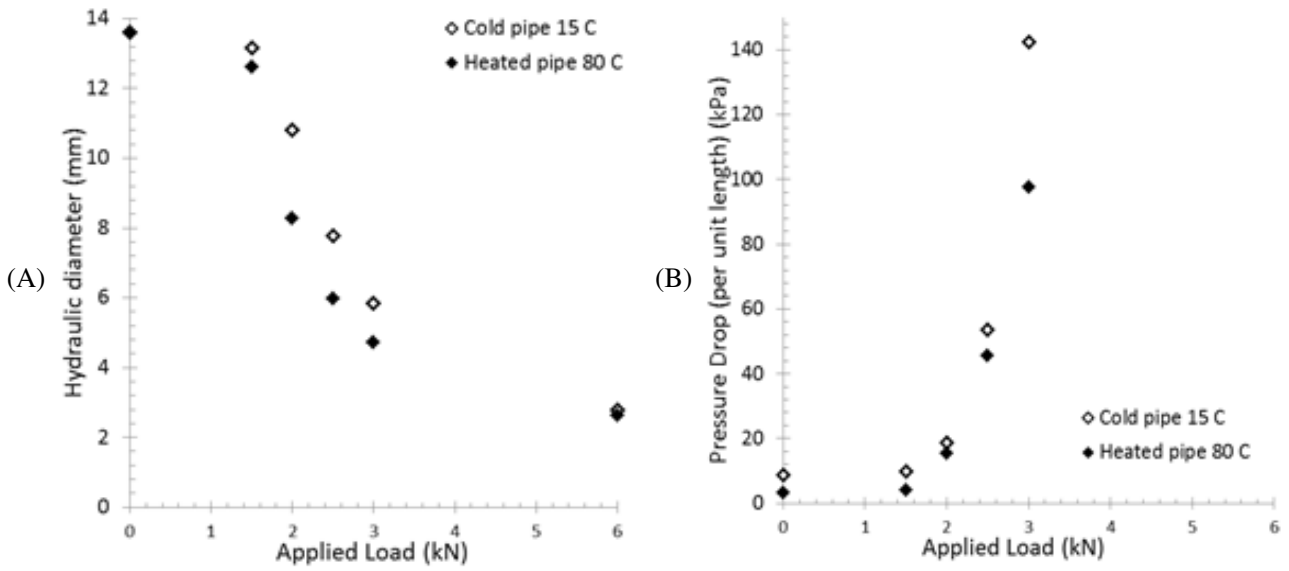

Figure 11. **(A)** graph showing the theoretically calculated hydraulic diameter, and **(B)** graph showing the theoretically calculated Pressure drop, for differing applied loads

References

[1] Petersen Products Co., 421 Wheeler Ave, Fredonia, WI 53021-0340, US, 2017.

[2] Copper Development Association Inc.

[3] Canadian Copper and Brass Development Association, Toronto, M4H 1P1, Canada, 2019.

[4] Dick RJ, Wray JA and Johnston HN. A Literature and Technology Search on the Bacteriostatic and Sanitizing Properties of Copper and Copper Alloy Surfaces, Phase 1 Final Report, INCRA Project No. 212, June 29, 1973, contracted to Battelle Columbus Laboratories, Columbus, Ohio.

[5] Minnesota Department of Health, 625 North Robert Street, St Paul, Minnesota.

[6] Wednesbury Copper Tube, Mueller Europe Ltd, Oxford Street, Bilston, WV14 7DS, UK.

[7] Fateh A, Aliofkhazraei M and Rezvanian AR. Review of corrosive environments for copper and its corrosion inhibitors. Arabian journal of Chemistry, In press, 2017. https://doi.org/10.1016/j.arabjc.2017.05.021

[8] Materials Data Handbook, Cambridge University Engineering Department, UK, 2003 Edition, 13.

[9] Dubreuil A, Young SB, Atherton J, *et al*. Metals recycling maps and allocation procedures in life cycle assessment. The International Journal of Life Cycle Assessment, 2010, **15**(6): 621-634. https://doi.org/10.1007/s11367-010-0174-5

[10] Amos J. Waste and Recycling. Heinemann Raintree, 1993.

[11] ASM Metal Recycling, The Recycling Centre, Aylesbury, Bucks, HP19 8BB, UK.

[12] Kundig KJA. Copper Applications in plumbing. Copper Development Association, 1998.

[13] Miller R. Making Seamless tubing with a floating mandrel mill. Tube and Pipe Journal, 2000.

[14] Chapman DSC. Effect of process variables on the tube drawing process and product integrity, Master's Thesis, Texas Tech University, USA, 1991.

[15] DeGarmo EP, Black JT and Kohser RA. Materials and Processes in Manufacturing, Wiley, 2003.

[16] Lide DR. CRC Handbook of Chemistry and Physics. 84th Edition, CRC Press, Florida, USA, 2004.

[17] Katsareas DE. Finite Element Simulation of Welding in Pipes: A sensitivity analysis. Residual stress and its effect of fracture, Springer, Dordrecht, 2006: 15-26. https://doi.org/10.1007/1-4020-5329-0_2

[18] Yaghi A, Hyde TH, Becker AA, *et al*. Residual stress simulation in thin and thick-walled stainless steel pipe welds including pipe diameter effects. The International Journal of Pressure Vessels and Piping, 2006, **83**(11-12): 864-874. https://doi.org/10.1016/j.ijpvp.2006.08.014

[19] Yaghi AH, Hyde TH, Becker AA, *et al*. Finite element simulation of welding residual stresses in martensitic steel pipes. Materials Research Innovations, 2013, **17**(5): 306-311. https://doi.org/10.1179/1433075X13Y.0000000140

[20] Zhou Y, Chen XD, Fan ZC, *et al*. Finite Element Modelling of Welding Residual Stress and Its Influence on Creep Behavior of a 2.25Cr-1Mo-0.25V Steel Cylinder. Procedia Engineering, 2015, **130**: 552-559. https://doi.org/10.1016/j.proeng.2015.12.264

[21] Siddique M, Abid M, Junejo HF, *et al*. 3-D Finite Element Simulation of Welding Residual Stresses in Pipe-Flange Joints: Effect of Welding Parameters. Materials Science Forum, 2005, **490-491**: 79-84. https://doi.org/10.4028/www.scientific.net/MSF.490-491.79

[22] Mohammad R. Impact loading and transient response of pipes transporting gas / liquid, University of Adelaide. PhD Thesis, 2011.

[23] Kwan A, Ng PL and Lam JY. Potential underground pipe failure due to load concentration at pipe crossings, The First International Conference on Utility Management and Safety, Hong Kong, China, 2009.

[24] Scientific Forming Technologies Corporation, 2545 Farmers Drive, Columbus, Ohio 43235, USA.

[25] Moody L. Friction Factors for pipe flow. Transactions of the ASME, 1944, **66**(8): 671-684.

[26] Acheson DJ. (1990), Elementary Fluid Dynamics, Oxford University Press, Oxford, UK, 1990.

[27] Ramanujan S . Modular equations and approximations to π. Also in Collected Papers of Srinivasa Ramanujan, Gh Hardy, Pv Seshu Aiyar, & Bm. 1914. https://doi.org/10.1007/978-1-4757-4217-6_29

[28] White FM. Fluid Mechanics (7^{th} Ed.), MacGraw-Hill Asia, 2011.

[29] Greenwood NN and Earnshaw A. Chemistry of the Elements (2^{nd} Ed.), Butterworth-Heinemann, 1997.

[30] Rumble JR. CRC Handbook of Chemistry and Physics (99^{th} Ed.). Boca Raton, FL: CRC Press, 2018